



Original Paper

Fracture sealing performance of granular lost circulation materials at elevated temperature: A theoretical and coupled CFD-DEM simulation study



Chong Lin^{a, b}, Qi-Cong Xu^a, Lie-Xiang Han^a, Gao Li^b, Hai He^a, Hong-Ling Zhou^{c, *}, Ji-Ping She^{d, e}

^a CCDC Drilling & Production Technology Research Institute, Guanghan, 618300, Sichuan, China

^b State Key Laboratory of Oil and Gas Reservoir Geology and Exploitation, Southwest Petroleum University, Chengdu, 610500, Sichuan, China

^c College of Materials Science and Engineering, Chongqing University, Chongqing, 400044, China

^d State Key Lab of Oil and Gas Reservoir Geology and Exploitation (Chengdu University of Technology), Chengdu, 610059, Sichuan, China

^e College of Energy, Chengdu University of Technology, Chengdu, 610059, Sichuan, China

ARTICLE INFO

Article history:

Received 11 November 2022

Received in revised form

1 October 2023

Accepted 1 October 2023

Available online 9 October 2023

Edited by Jia-Jia Fei

Keywords:

Geothermal well drilling

HTHP formation

Lost circulation material

CFD-DEM

Fracture sealing

ABSTRACT

Lost circulation is a common downhole problem of drilling in geothermal and high-temperature, high-pressure (HTHP) formations. Lost circulation material (LCM) is a regular preventive and remedial measure for lost circulation. However, conventional LCMs seem ineffective in high-temperature formations. This may be due to the changes in the mechanical properties of LCMs and their sealing performance under high-temperature conditions. To understand how high temperature affects the fracture sealing performance of LCMs, we developed a coupled computational fluid dynamics-discrete element method (CFD-DEM) model to simulate the behavior of granular LCMs in fractures. We summarized the literature on the effects of high temperature on the mechanical properties of LCMs and the rheological properties of drilling fluid. We conducted sensitivity analyses to investigate how changing LCM slurry properties affected the fracture sealing efficiency at increasing temperatures. The results show that high temperature reduces the size, strength, and friction coefficient of LCMs as well as the drilling fluid viscosity. Smaller, softer, and less frictional LCM particles have lower bridging probability and slower bridging initiation. Smaller particles tend to form dual-particle bridges rather than single-particle bridges. These result in a deeper, tighter, but unstable sealing zone. Reduced drilling fluid viscosity leads to faster and shallower sealing zones.

© 2023 The Authors. Publishing services by Elsevier B.V. on behalf of KeAi Communications Co. Ltd. This is an open access article under the CC BY-NC-ND license (<http://creativecommons.org/licenses/by-nc-nd/4.0/>).

1. Introduction

Geothermal energy, an important renewable energy resource, especially for off-grid locations, has received increasing attention in recent decades because of its renewability, cleanliness, low-carbon emission, safety and ubiquity. Therefore, geothermal energy can be an alternative to traditional fossil energy and a supplement to the growing energy consumption worldwide. Geothermal wells have been the most effective technique for obtaining geothermal energy from underground to the surface. However, drilling the well is the primary element in the cost of geothermal energy application.

Moreover, lost circulation has been a major factor in increasing the costs for drilling and completion in geothermal wells because of high temperatures (from 160 to over 300 °C), hard formation rocks (compressive strength over 240 MPa), highly fractured (fracture apertures on the order of centimeters) and underpressured situations. Lost circulation treatments may represent 15% of the total well cost (Finger and Blankenship, 2010). It can also lead to troublesome, unsafe and costly consequences, such as drilling fluid loss, significant downtimes, stuck pipe, wellbore instability, well kicks, incomplete primary cement operations and, in extreme cases, well abandonment. The treatment for these issues can be challenging and costly (Pierce and Livesay, 1994).

Lost circulation materials (LCMs), cementing, blind drilling and underbalanced drilling are the most common methods to control

* Corresponding author.

E-mail address: zhouhongling@cqu.edu.cn (H.-L. Zhou).

lost circulation during geothermal drilling and completion. LCMs are regularly added to the drilling fluid to prevent lost circulation before entering the loss zone. They are also a primary treatment after lost circulation occurs (Alsaba et al., 2014a). However, most of the LCMs developed and used in oil and gas drilling have proven little or no use because of the unpredictable nature of the fractures (with widths on the order of centimeters), the complicated movement of LCM particles, and the change in the mechanical properties of LCMs at elevated temperatures (Loeppke et al., 1990; Visser et al., 2014). Nevertheless, LCMs are still the first choice for drilling engineers treating lost circulation problems because they are less time-consuming, have low equipment requirements and are low cost. Moreover, it is better to use LCMs to temporarily seal the pay zones instead of permanently sealing them with cement (Finger and Blankenship, 2010). It is noteworthy that LCMs can be added to the cement slurry to cure severe lost circulation events induced by large fractures.

Three typical LCMs are used in geothermal drilling: fibrous, flaky and granular. Fibrous and flaky LCMs bridge the fracture and transform it into a porous structure, which traps the subsequent LCMs. Granular LCMs form a porous bridge that gradually reduces the permeability of the sealing zone (Nugroho et al., 2017). Mica flakes added to cement slurry have proven to be an effective remedy for induced or natural fractures causing lost circulation (Visser et al., 2014). To understand the factors influencing the fracture sealing performance of LCM slurry, extensive laboratory experiments and numerical simulations were conducted. The fracture sealing process was found to be affected by the LCM type, combination, size distribution, shape, concentration, friction coefficient, and elasticity and by the drilling fluid type, density, viscosity and injection rate/pressure (Alsaba et al., 2014b; Feng et al., 2018; Bao et al., 2019b; Ettehadi et al., 2019; Xu et al., 2019a; Savari et al., 2012; Kaageson-Loe et al., 2009). Lin et al. (2022) noted in their numerical simulations that the particle size, Young's modulus, friction coefficient and concentration of the LCM determine whether fracture sealing initiates. However, the fracture sealing performance of LCM seems to be sensitive to temperature. The sealing width and strength of LCMs are significantly reduced at high temperatures (Alsaba et al., 2014b; Jeennakorn et al., 2019). This may be attributed to the degradation of the size, strength, friction coefficient and resilience of LCMs after high-temperature aging (Kang et al., 2019b; Bao et al., 2019a). Unfortunately, although it is widely accepted that high temperature affects the fracture sealing ability of LCMs, how the properties of LCMs change at elevated temperatures and how these changes affect fracture sealing are still unclear.

In this study, we developed a coupled CFD-DEM model to simulate the behavior of granular LCMs in sealing fractures. The viscosity of the drilling fluid, particle size, friction coefficient, Young's modulus, and Poisson's ratio of LCMs were varied to represent a range of conditions under the geothermal temperature range. A series of sensitivity analyses were conducted to investigate the sealing efficiency of LCMs in fractures for temperatures up to 300 °C. We attempted to understand the mechanisms behind the failure of conventional LCMs in high-temperature environments.

2. Effect of elevated temperature on basic properties of LCMs and drilling fluid

The viscosity of the drilling fluid is strongly influenced by temperature. The apparent viscosity of the drilling fluid decreases with increasing temperature, regardless of the base fluid. However, the plastic viscosity of the drilling fluid initially decreases and then slightly increases with increasing temperature (Santoyo et al., 2001; Zhao et al., 2008; Wang et al., 2012; Amani and Al-jubouri,

2012). Table 1 shows the variation of viscosity for different drilling fluids at elevated temperatures. As the temperature rises above 200 °C, the viscosity of the drilling fluids decreases significantly at shear rates of 1022 and 511 s⁻¹. The drilling fluid can reach the lowest viscosity of 0.25 mPa·S at a shear rate of 170 s⁻¹ at high temperature (Santoyo et al., 2001). The rheological parameters better characterize the non-Newtonian rheology of drilling fluids than the apparent viscosity and plastic viscosity. A water-based drilling fluid exhibits an increasing flow behavior index and a decreasing consistency index at elevated temperature (up to 180 °C) (Zhu et al., 2020) (see Table 2).

LCMs undergo a series of environmental changes and physical and chemical reactions during the transport process from the ground to the loss zone, such as increased temperature and pressure, drilling fluid immersion, high-speed shearing, collision between particles and flow boundaries and collision between particles. These factors can promote the abrasion of LCMs. Experimental studies have shown that walnut shells, graphite, marble granules, calcium carbonate, and other common LCMs experience a significant reduction in particle size under a specific shear rate in the drilling fluid at high temperatures for half to one day (Scott et al., 2012; Valsecchi, 2014; Yang, 2015; Grant, 2016). Kang et al. (2019a) demonstrated through experiments that the size degradation of granular calcium carbonate by abrasion is slightly sensitive to the fluid temperature (80–160 °C). Their subsequent work revealed that walnut shell and millimeter-scale granular calcium carbonate suffer both quality and size loss after heating to 180 °C in an oil-based drilling fluid (Kang et al., 2019b). The experimental results of Klungtvedt and Saasen (2022) indicated that calcium carbonate has the largest particle size degradation, followed by resilient graphite and the smallest granular cellulose. Decreasing fluid viscosity can increase the size degradation rate (Kumar et al., 2013). Therefore, the size degradation of LCMs may be exacerbated at elevated temperatures because of the decreased viscosity of the fluid.

The temperature sensitivity of the mechanical properties of geomaterials has been reported. The compressive strength, friction coefficient, Young's modulus, and Poisson's ratio are the most critical and typical mechanical properties of LCMs. The experimental results of carbonate (limestone and marble) indicate that these properties decrease at elevated temperatures (Fig. 1). The uniaxial compressive strength decreases from 120 to 86 MPa, the elastic modulus decreases from 22 to 7 GPa, and Poisson's ratio decreases from 0.3 to 0.1 after heating to 300 °C (Zhang et al., 2009; Brotóns et al., 2013). Kang et al. (2019b) observed that the friction coefficient of walnut shells and calcium carbonate decreases to 28% and 1% of the initial value, respectively, after heating to 180 °C. Carbonate is the natural source of calcium carbonate, which is the most popular LCM used in drilling operations. Therefore, the temperature-induced degradation of the mechanical properties of LCMs is a serious concern.

3. Methodology

3.1. Description of the problem

The objective of this study is to simulate the flow of LCM-laden drilling fluid and the behavior of granular LCMs in sealing a simplified vertical fracture. We mainly examine the effect of temperature-induced variations in mechanical properties on the sealing process. The fracture geometry used here is a vertical wedge, as illustrated in Fig. 2. The fracture is 100 mm long and 25.4 mm high, with a linearly decreasing width from 1 mm at the inlet to 0.34 mm at the outlet. We assumed that the formation is stiff, so the fracture walls are modeled as rigid smooth surfaces,

Table 1
Variation of drilling fluid viscosity at elevated temperatures.

Drilling fluid	Density, g/cm ³	Temperature, °C	Viscosity at 1022 s ⁻¹ , mPa·s	Viscosity at 511 s ⁻¹ , mPa·s	References
Fresh water-based	2.2	50–220	640–126	328–75	Wang et al. (2012)
Brine-based	2.2	50–220	235–89–110	125–55–44.5	
Geothermal spring water-based	1.03	15–150	(22.4–39.4)–(3.8–17.2)	(16.4–28.7)–(1.5–10.5)	Avci and Mert (2019)
2# Diesel-based	1.32	23.9–204.4	(106–334)–(12–34)	(63–190)–(9–22)	Yan and Zhao (2003)
Mentor26 mineral oil-based	1.32	23.9–204.4	(160–434)–(24–58)	(102–267)–(17–40)	

Table 2
Size degradation of LCM particles at elevated temperatures.

LCM	Rotation speed, rpm	Time, min	Fluid	Temperature, °C	D ₉₀ , μm	Size degradation rate, %	References
Calcium carbonate	1000	30	Water-based fluid	80	44.153	35.80	Kang et al. (2019a)
				100	44.153	35.37	
				120	44.153	34.40	
				120	16.435	10.57	
				120	27.765	28.75	
				120	201.431	45.05	
				120	510.447	59.46	
				140	44.153	33.40	
				160	44.153	33.54	
				160	44.153	33.54	
Calcium carbonate Graphitic carbon Walnut	4000	30	Xanthan viscosifier solution	49	300–1400	5–80	Kumar et al. (2013)
					700–1250	14–17	
					900	1	

although the fracture roughness may facilitate the bridging process. Therefore, this model can be a simplified representation of a part or the whole of a realistic subsurface fracture.

3.2. Basic theory of CFD-DEM

The behavior of granular LCMs to seal a fracture is simulated by the coupled CFD-DEM model developed based on CFDEM@coupling, an open-source CFD-DEM engine (Kloss et al., 2012; Hager et al., 2018). The unresolved CFD-DEM approach is adopted here because the simulation may involve approximately 100,000 LCM particles (Hager, 2014). In the CFD-DEM, the movement of an incompressible fluid with particles is governed by the volume-averaged Navier-Stokes equations (Zhou et al., 2010).

$$\frac{\partial(\varepsilon_f)}{\partial t} + \nabla \cdot (\varepsilon_f \mathbf{u}_f) = 0 \quad (1)$$

$$\frac{\partial(\rho_f \varepsilon_f \mathbf{u}_f)}{\partial t} + \nabla \cdot (\rho_f \varepsilon_f \mathbf{u}_f \mathbf{u}_f) = -\varepsilon_f \nabla p - \mathbf{F}_{pf} + \varepsilon_f \nabla \cdot \boldsymbol{\tau} + \rho_f \varepsilon_f \mathbf{g} \quad (2)$$

$$\mathbf{F}_{pf} = \frac{1}{\Delta V} \sum_{i=1}^n (\mathbf{f}_{d,i} + \mathbf{f}_i'') \quad (3)$$

$$\mathbf{f}_{pf,i} = \mathbf{f}_{d,i} + \mathbf{f}_{\nabla p,i} + \mathbf{f}_{\nabla \cdot \boldsymbol{\tau},i} + \mathbf{f}_i'' \quad (4)$$

where ε_f is the fluid volume fraction (dimensionless), t is the time (s), \mathbf{u}_f is the fluid velocity (m/s), ρ_f is the fluid density (kg/m³), p is the fluid pressure (Pa), \mathbf{F}_{pf} and \mathbf{f}_{pf} are fluid-particle interaction forces (N), $\boldsymbol{\tau}$ is the stress tensor, \mathbf{g} is the gravitational acceleration (m/s²), ΔV is the cell volume (m³), n is the number of particles, \mathbf{f}_d is the drag force (N), $\mathbf{f}_{\nabla p}$ (including the buoyancy force) is the pressure gradient force (N), $\mathbf{f}_{\nabla \cdot \boldsymbol{\tau}}$ is the viscous force (N), and \mathbf{f}_i'' is the sum of other particle-fluid interaction forces (N), including the virtual mass force, Basset force, Saffman lift force and Magnus force (Crowe et al., 2011). \mathbf{F}_i'' are neglected because \mathbf{f}_d , $\mathbf{f}_{\nabla p}$ and $\mathbf{f}_{\nabla \cdot \boldsymbol{\tau}}$ are dominant among all fluid-particle interactions in this paper's situation (Zhou et al., 2010; Poia et al., 2017).

The Di Felice model (Eqs. (5)–(8)) (Di Felice, 1994) is used here because it is suitable for both dilute and dense particle flow. It accurately matches the experimental terminal velocity over a wide range of Reynolds numbers. Moreover, it has the advantage of correcting the drag force by considering the effect of the surrounding particles.

$$\mathbf{f}_{d,i} = \frac{C_d}{24} Re_{p,i} \varepsilon_f^{-x} \quad (5)$$

$$x = 2.7 - 0.65 e^{[-0.5(1.5 - \log_{10} Re_{p,i})^2]} \quad (6)$$

$$C_d = (0.63 + 4.8 Re_{p,i}^{-0.5})^2 \quad (7)$$

$$Re_p = \frac{|\mathbf{u}_f - \langle \mathbf{u}_p \rangle| d_p}{\nu_f} \quad (8)$$

where Re_p is the particle Reynolds number (dimensionless), C_d is the drag force (N), $\langle \mathbf{u}_p \rangle$ is the averaged particle velocity in a cell (m/s), d_p is the particle diameter (m), and ν_f is the fluid kinematic viscosity (m²/s).

The DEM computes the movement of each particle by considering the effects of other particles, walls or forces. The motion of a particle comprises translation and rotation. According to Newton's second law, the translational governing equation for a particle is

$$m_p \frac{d\mathbf{u}_p}{dt} = m_p \mathbf{g} + \sum_{N_p} \mathbf{F}_{pp} + \sum_{N_w} \mathbf{F}_{pw} \quad (9)$$

where m_p is the particle mass (kg), N_p is the number of particles, \mathbf{F}_{pp} is the particle-particle interaction force (N), N_w is the number of walls, and \mathbf{F}_{pw} is the particle-wall interaction force (N).

The rotational governing equation of a particle is

$$I_p \frac{d\boldsymbol{\omega}_p}{dt} = T_p + T_r \quad (10)$$

where I_p is the inertial tensor (kg·m²), $\boldsymbol{\omega}_p$ is the angular velocity

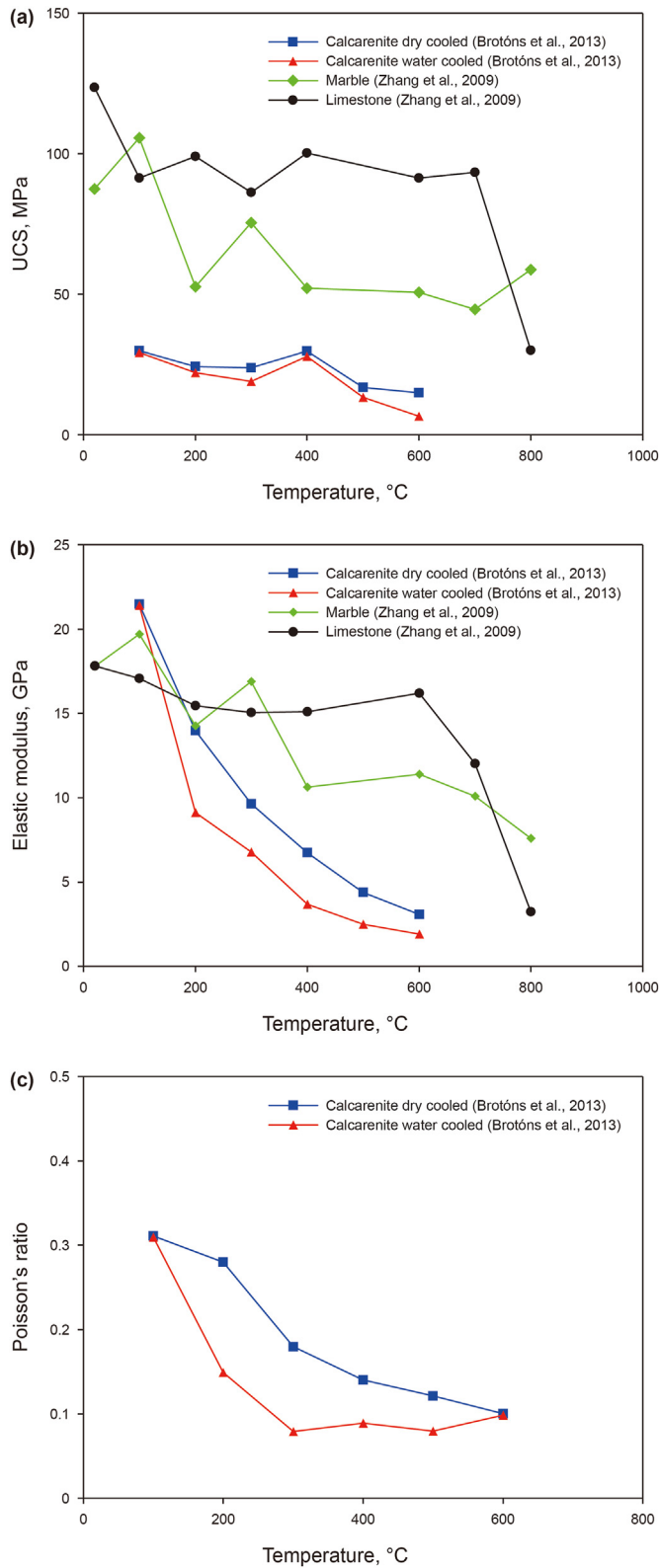


Fig. 1. Variation of mechanical properties of carbonate rocks at elevated temperatures: (a) uniaxial compressive strength (UCS); (b) elastic modulus; and (c) Poisson's ratio.

(rad/s), T_p is the torque (N·m), and T_r is an additional torque on the particle that can model nonsphericity by a rolling friction model (N·m).

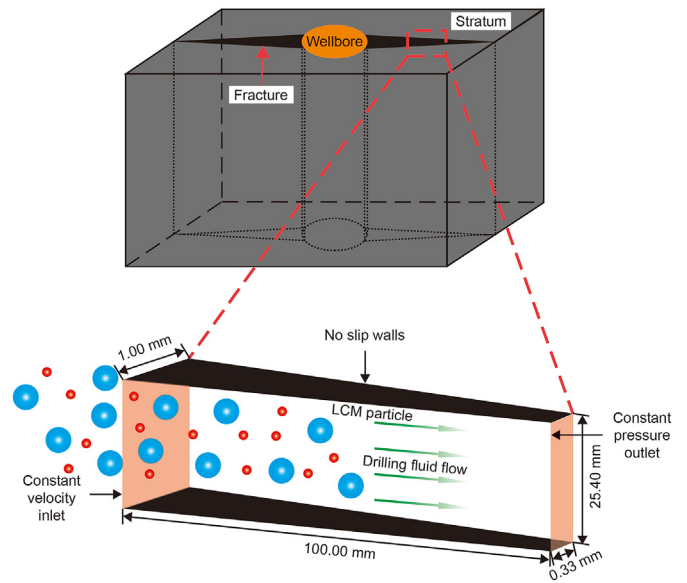


Fig. 2. Schematic representation of the vertical wedge-shaped fracture and boundary conditions.

The F_{pp} and F_{pw} in Eq. (9) are contact forces. They are generated when either a particle collides with another particle or a particle collides with the wall. The soft sphere model is applied here because of its advantages in representing collisions in dense particle systems. In soft models, nonlinear force-displacement models are more accurate than linear spring-dashpot models, especially in dense particle systems where interparticle interactions dominate (Wellmann et al., 2008; Norouzi et al., 2016). During LCM slurry placement in the fracture, particle-particle interactions play an important role because of their high concentration. Therefore, the nonlinear viscoelastic Hertz contact model is used here to represent the contact forces of LCM particles.

$$F_{pp} = (k_n \delta_{n_{ij}} - \gamma_n u_{n_{ij}}) + (k_t \delta_{t_{ij}} - \gamma_t u_{t_{ij}}) \quad (11)$$

where k is the elastic constant (N/m), δ is the overlap distance (m), γ is the viscoelastic damping constant (N·s/m), and u is the relative velocity (m/s). The subscripts n and t denote the normal and tangential directions, respectively.

The elastic constants and viscoelastic damping constants in Eq. (11) depend on the overlap distance between particles. Their relationships are given by Eqs. (12)–(19).

$$k_n = \frac{4}{3} E^* \sqrt{R^* \delta_n}, k_t = 8G^* \sqrt{R^* \delta_t} \quad (12)$$

$$\delta_n = R_1 + R_2 - |\vec{x}_2 - \vec{x}_1|, \delta_t = \int_{t_0}^t u_t dt \quad (13)$$

$$\gamma_n = -2\sqrt{\frac{5}{6}} \beta \sqrt{S_n m^*} \geq 0, \gamma_t = -2\sqrt{\frac{5}{6}} \beta \sqrt{S_t m^*} \geq 0 \quad (14)$$

$$S_n = 2E^* \sqrt{R^* \delta_n}, S_t = 8G^* \sqrt{R^* \delta_t} \quad (15)$$

$$\beta = \frac{\ln(e)}{\sqrt{\ln^2(e) + \pi^2}} \quad (16)$$

$$\frac{1}{E^*} = \frac{(1 - \nu_1^2)}{E_1} + \frac{(1 - \nu_2^2)}{E_2} \quad (17)$$

$$\frac{1}{G^*} = \frac{2(2 - \nu_1)(1 + \nu_1)}{E_1} + \frac{2(2 - \nu_2)(1 + \nu_2)}{E_2} \quad (18)$$

$$\frac{1}{R^*} = \frac{1}{R_1} + \frac{1}{R_2}, \frac{1}{m^*} = \frac{1}{m_1} + \frac{1}{m_2} \quad (19)$$

where E is Young's modulus (Pa), R is the radius (m), \vec{x} is the position vector, m is the mass (kg), ν is Poisson's ratio (dimensionless), and e is the coefficient of restitution of the particle (dimensionless).

3.3. Basic parameter setup of the numerical model

The CFD domain is divided into hexahedral mesh cells with dimensions of 2 mm × 2 mm × (0.34–1) mm. The characteristic length of a single mesh cell is at least 3 times the diameter of the particle, which ensures accurate and convergent results (Peng et al., 2015). This size also ensures that the porosity changes smoothly. The boundary conditions at the inlet, outlet and fracture walls are a constant injection rate, a constant pressure and a no-slip wall, respectively. A linear velocity of 1 m/s along the fracture direction is the initial velocity condition at the inlet. The pressure at the outlet is zero. Gravity is 9.81 m/s² downward along the height of the fracture. Other field data are calculated based on these velocity and pressure field data. The Reynolds number is a dimensionless parameter that indicates whether the flow is laminar or turbulent. According to the Reynolds number of the noncircular duct calculated by the hydraulic diameter, the Reynolds number in our study is less than 100, which indicates laminar flow inside the fracture. Although drilling fluids are typically non-Newtonian fluids, the shear thinning behavior can be approximated as Newtonian fluids because of the relatively low flow rate in this problem. Thus, the drilling fluid flow is treated as a laminar flow of an incompressible Newtonian fluid. The time steps of CFD and DEM are 10⁻⁵ and 10⁻⁷ s, respectively. Therefore, CFD and DEM couple once every 100 DEM time steps. These time steps satisfy all criteria of the Courant number for CFD calculation, Hertz time, Rayleigh time and particle relaxation time for DEM calculations, and response time of fluid and particle.

A series of simulations are conducted to understand the effect of mechanical property variations at elevated temperatures on the fracture sealing process. The basic parameters of the simulation are shown in Table 3.

3.4. Model validation

The model validation is based on the experimental result of single sphere sedimentation and the analytical result of pressure drop through a random particle bed under steady state fluid flow. They represent the cases where the particle-particle interaction forces are negligible and significant, respectively (Sun et al., 2018).

Single-sphere sedimentation is a classical problem of dilute particle flow. Concha (2009) derived a sedimentation velocity equation of a sphere and validated it by experimental data from Lapple and Shepherd (1940). Two more results of the settling experiment of a spherical particle (Chakraborti and Kaur, 2014; Rushd et al., 2019) are used for further validation of Concha's equation. Fig. 3 shows that the experimental data of these two studies agree well with the equation. This proves that Concha's equation has good applicability for a wide range of sphere sizes. A series of sphere sedimentation simulations are performed using our developed model. The box has a size of 25 d_p × 25 d_p × 250 d_p . The sphere starts to settle from the center of the top face at a height of approximately 240 d_p . Six sizes of spherical particles with Reynolds numbers ranging from 10⁻⁵ to 10³ are simulated. The results show that the error between our simulated data and the experimental data is 2.00%–16.91%, with an average of 8.05%. Fig. 3 shows that the results of our numerical simulation also agree well with Concha's equation. The error between our simulated data and Concha's equation data is 0.56%–15.31%, with an average of 7.30%. This result is comparable to the error between the Concha equation data and experimental data (0.15%–10.96%, average of 4.29%). The above results validate that our numerical model is applicable for the problem of dilute particle flow, where the particle-particle interactions are negligible.

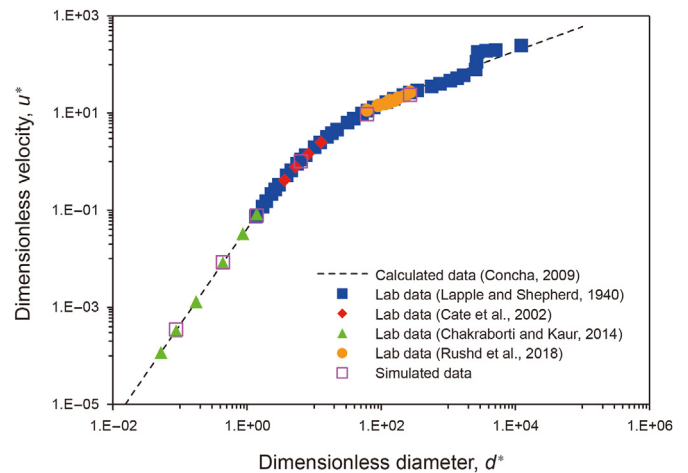


Fig. 3. Model validation results for the settling velocity of a single sphere.

Table 3
Simulation parameters for the fluid phase and particle phase.

Phase	Property parameter	Value
Fluid	Density, kg/cm ³	1700
	Dynamic viscosity, Pa·s	0.0001/0.001/0.01/0.05/0.1/0.15
Particle	Density, kg/cm ³	2700
	Diameter, mm	0.1/0.2/0.33/0.4/0.5/0.6/0.7/0.8/0.9/1.0
	Young's modulus, GPa	0.1/1/10/30/50/70/100
	Poissons ratio	0.1/0.2/0.3/0.4/0.5
	Restitution coefficient	0.5
	The friction coefficient of particles	0/0.2/0.4/0.6/0.8/1.0
	The friction coefficient of particle and fracture surface	0/0.2/0.4/0.6/0.8/1.0

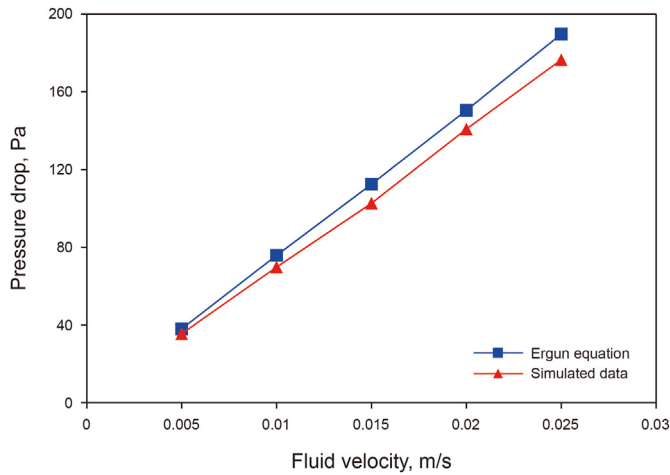


Fig. 4. Comparison of model calculations and Ergun equation for the pressure drop across a random particle bed.

Fracture sealing by LCM particles is a problem of dense particle flow where particle-particle interactions dominate. Therefore, a classical problem of dense particle flow, pressure drop through a random particle bed, is also simulated for our model validation. The equation for a pressure drop of fluid flow through a sphere bed given by Ergun (1952) is:

$$\frac{\Delta P}{L} = \frac{150\mu_f V_0}{d_p^2} \cdot \frac{(1 - \epsilon)^2}{\epsilon^3} + \frac{1.75\rho_f V_0^2}{d_p} \cdot \frac{(1 - \epsilon)}{\epsilon^3} \quad (20)$$

where Δp is the pressure drop of the sphere bed (Pa), L is the length of the sphere bed (m), μ_f is the viscosity of the fluid (mPa·S), V_0 is the superficial velocity of the fluid (m/s), and ϵ is the voidage of the sphere bed.

The pressure drop results of the fluid flow through the random particle bed are shown in Fig. 4. The random particle bed has a size of $\Phi 13.8 \text{ mm} \times 15 \text{ mm}$ and consists of 10,000 spheres of 1 mm diameter. The voidage is 42%. The fluid viscosity is 15 mPa·S. The CFD domain has a geometry of $\Phi 13.8 \text{ mm} \times 55.3 \text{ mm}$. Constant flow velocity fluid is injected from the bottom, and the Reynolds number is below 1 to ensure laminar flow. The top outlet pressure is constant at 10 Pa. As shown in Fig. 4, the error between the simulation results and analytical results is less than 10%. This indicates that the proposed model is suitable for the problem of dense particle flow, where the particle-particle interactions are significant.

4. Results and discussion

4.1. Effect of thermally induced viscosity reduction of drilling fluid on fracture sealing

The effect of drilling fluid viscosity (μ) reduction at elevated temperatures on the formation of a sealing zone by LCMs is significant, as shown in Figs. 5 and 6. The volume concentration of the LCMs is 10% in all simulations. A sealing situation occurs when particles stop and accumulate in a cross-section of the fracture, and the pressure of the fracture inlet increases simultaneously. First, the drilling fluid viscosity reduction changes the velocity of the LCM particles at high temperatures. In low-viscosity drilling fluid, LCM particles move faster but with a lower local concentration than in high-viscosity drilling fluid. LCM particles travel further and bridge faster at low viscosity (Fig. 5). However, the settlement of particles in the fracture is negligible because of the insertion velocity,

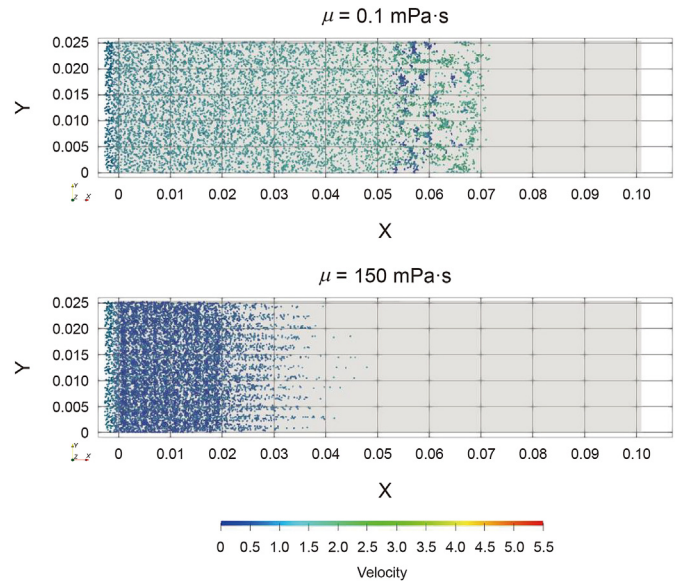


Fig. 5. Effect of drilling fluid viscosity on the motion and bridging of LCM particles in a fracture. The snapshots show the LCM particles after 0.6–0.8 V_{fracture} (volume in the fracture) drilling fluid is injected. The LCM particles tend to move along the fracture length direction with few particle bridges in low-viscosity drilling fluid. The color of each particle indicates its velocity magnitude, which reflects its movement state. The velocity decreases as the color gradually changes from red to blue.

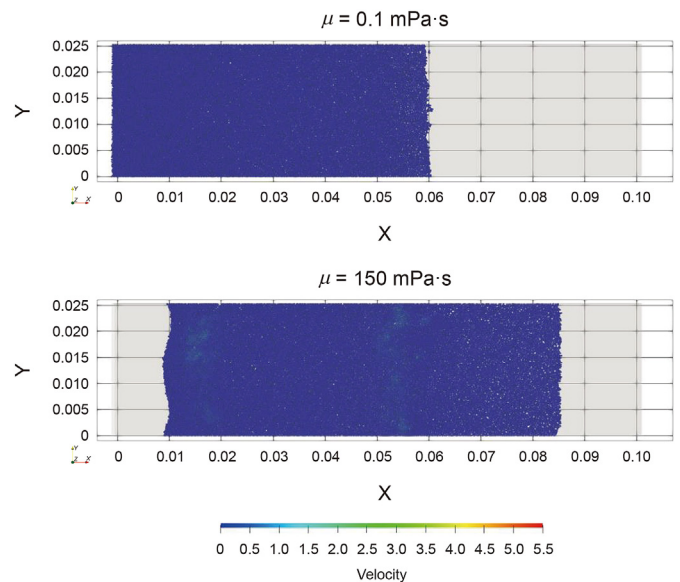


Fig. 6. Fracture sealing state of LCMs under different drilling fluid viscosities after approximately 10 V_{fracture} drilling fluid is injected. The dark blue color indicates that the particles are immobile under the drilling fluid flow, which implies a successful seal.

fracture length and particle concentration. A reduction in the drilling fluid viscosity significantly shortens the sealing zone depth, and sealing occurs earlier inside the fracture. When the viscosity of the drilling fluid decreases from 150 to 0.1 mPa·S, the sealing zone depth decreases initially and then changes little after 10 mPa·S (Fig. 6). The results of $\mu = 0.1$ and 1 mPa·S are similar, while the results of $\mu = 10, 50, 100$ and 150 mPa·S are similar. Notably, the viscosity of the particle-laden fluid does not change with various volume fractions of particles in the unresolved CFD-DEM model (Blais et al., 2016). Therefore, the viscosity here is only the viscosity of the pure fluid phase.

The quality of the formed seal is also affected by the reduction in drilling fluid viscosity, in addition to the changes in the location of the formation of the sealing zone. Fig. 7(a) shows that both the maximum and the stable pressure difference between the inlet and outlet of the fracture decrease as the viscosity of the drilling fluid decreases. The pressure difference is 33 MPa at a viscosity of 150 mPa·S, while it decreases to 0.17 MPa at a viscosity of 0.1 mPa·S. According to the Kozeny-Carman equation (Carrier, 2003), the pressure difference of a laminar and steady-state fluid flow through a random particle bed is directly proportional to the viscosity of the fluid. However, the ratio of pressure difference is not equal to that of the corresponding viscosity. This means that other factors besides viscosity variation also impact the pressure difference variation. Simulation results show that the porosity of the sealing zone under decreasing drilling fluid viscosity is 0.461, 0.469, 0.481, 0.489, 0.477 and 0.475. The porosity increases as the viscosity decreases from 150 to 10 mPa·S and decreases as the viscosity decreases from 10 to 0.1 mPa·S. As the viscosity drops, the seal zone becomes looser. The flow rate at the fracture outlet continuously decreases from 2.50×10^{-5} to 1.16×10^{-5} m³/s as the viscosity of the drilling fluid decreases from 150 to 0.1 mPa·S (Fig. 7(b)). The cumulative drilling fluid volume passing through the fracture before sealing initially decreases and then slightly increases as the viscosity of the drilling fluid decreases. The smallest loss, i.e., the lowest cumulative drilling fluid volume, is obtained by the drilling fluid with a viscosity of 10 mPa·S (Fig. 7(c)). This trend is consistent with that of the porosity of the sealing zone. It is noticeable that major changes in the pressure difference, flow rate

and cumulative fluid loss volume occur when the viscosity of the drilling fluid decreases from 150 to 100 mPa·S. Below this limit, these three parameters change slightly with viscosity changes (Fig. 7(d)), as the viscosity of 150 mPa·S is high enough to continually destroy initially formed sealing zone and push it into deeper positions until a stable seal forms. Therefore, the outlet flow rate and cumulative fluid loss are much higher than those in the other cases. The large pressure difference results from combining the effect of the highest viscosity and flow rate of the drilling fluid and lowest porosity of sealing zone.

The simulation results show that the viscosity of the drilling fluid decreases as the temperature rises, which affects fracture sealing by the LCM. LCM particles bridge faster and form a shallower sealing zone with less fluid loss and a lower pressure difference in the fracture. A low viscosity of the drilling fluid means low resistance to particle movement. The particle can move faster to reach a suitable position to bridge in low-viscosity drilling fluid than in high-viscosity fluids. The reduction in drilling fluid viscosity seems to be positive for the rapid formation of the sealing zone. However, low-viscosity drilling fluids lead to more settlement of LCM particles at the fracture bottom. It is unfavorable for fracture sealing if the concentration of LCMs is lower than the critical value.

4.2. Effect of thermally induced particle size degradation on fracture sealing

Particle size is one of the essential properties of LCM design for sealing a fracture. Size degradation of LCM particles, which is driven

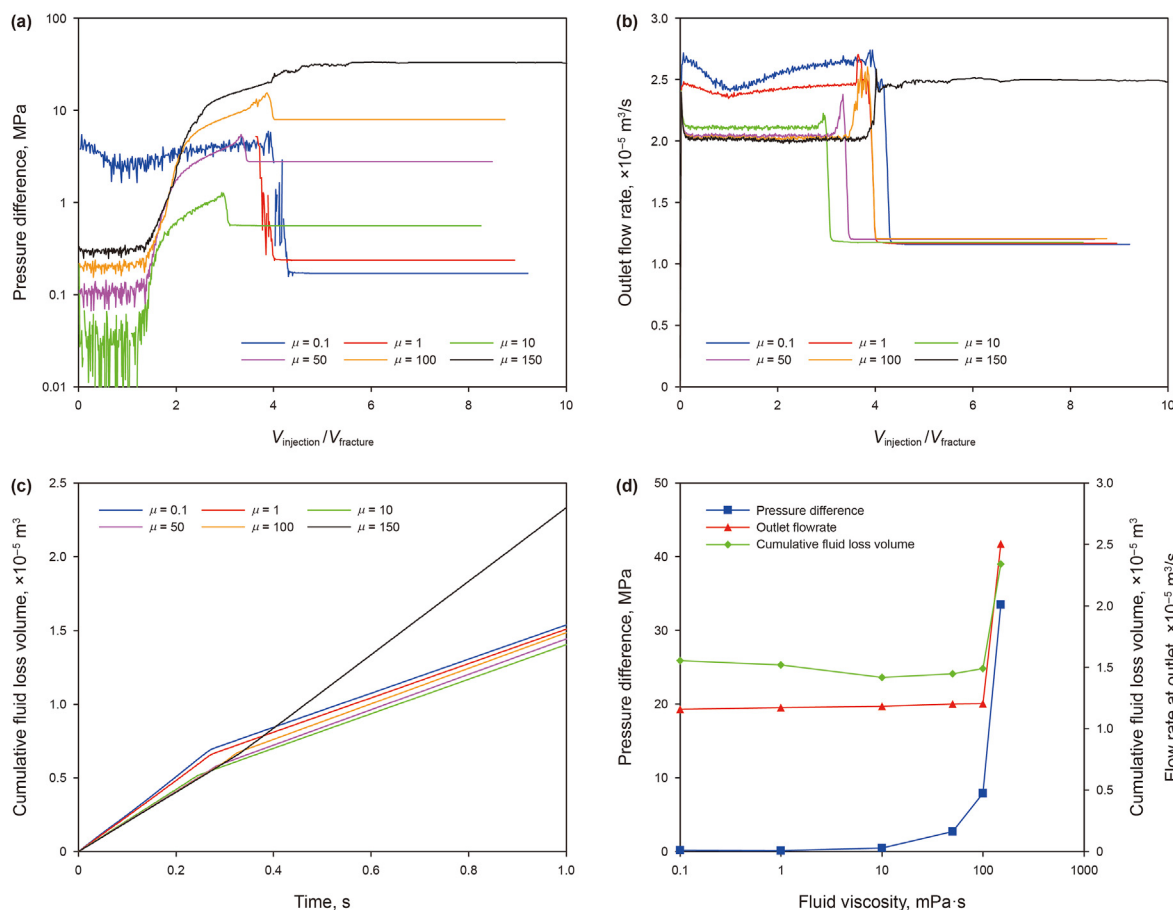


Fig. 7. Effect of drilling fluid viscosity on the flow parameters inside the fracture: (a) pressure difference; (b) outlet flow rate; (c) cumulative drilling fluid loss volume; and (d) flow parameter at the final state.

by thermal expansion rupture and thermal abrasion (Scott et al., 2012; Grant et al., 2016; Kang et al., 2019a), has a significant impact on fracture sealing efficiency. The particle size can be reduced to 20% of its original value in downhole elevated temperatures circulating in the environment. As shown in Fig. 8 (the last two figures) in the size range of 1.0–0.6 W_{fi} (fracture inlet width), the formation process of the sealing zone is dominated by the single-particle bridging mechanism. For particle diameter, $d_p = 1.0 W_{fi}$, LCM particles seal outside the inlet due to the wedge shape and size of the fracture. For $d_p = 0.6 W_{fi}$, LCM particles seal inside the fracture, which is similar to that of $d_p = 0.7, 0.8$ and $0.9 W_{fi}$. As the particle size decreases from 1.0 to 0.6 W_{fi} , both the bridging

initiation time and bridging depth increase. For $d_p = 0.4$ and $0.5 W_{fi}$, the sealing process is dominated by a dual-particle bridging mechanism in the near field and a single-particle bridging mechanism in the far field. The LCM particles bridge at a short distance from the inlet by the dual-particle bridging mechanism, and the escaping particles bridge again at a deeper position by the single-particle bridging mechanism, leaving a space between these two sealing zones (Fig. 8, middle figure). However, the stability of the sealing zone formed by the dual-particle bridging mechanism is weaker than that formed by the single-particle bridging mechanism. The initial bridging zone may collapse in the middle (Fig. 9). This may be because particles can more easily bridge at the top and bottom of the fracture, where three walls provide a sort of confinement for the particle flow. The later-coming particles pack at the previous bridge and gradually extend to the middle. Therefore, during the initiation of the sealing zone, the middle part is the weakest part. For LCM particle sizes less than $0.3 W_{fi}$, the process of sealing formation is dominated by a dual-particle bridging mechanism (Fig. 8, the first two figures). However, when the particle sizes are smaller than $0.2 W_{fi}$, the LCM particles cannot seal the fracture through the whole fracture height at this concentration. The formed incomplete sealing zone will eventually crash. When the dual-particle bridging mechanism works in the size range of 0.5 – $0.2 W_{fi}$, both the dual-particle bridging initiation time and bridging depth increase as the particle size decreases. Since the outlet width of the fracture is 0.34 mm, LCM particles smaller than $0.17 W_{fi}$ can barely bridge to seal the fracture.

The particle size also significantly influences the quality of the sealing zone (Fig. 10). When the particle size decreases from 1_i to $0.3 W_{fi}$, the pressure difference gradually increases except for $d_p = 0.5 W_{fi}$. This is because particles with $d_p = 0.5 W_{fi}$ form two thin sealing zones compared to the other particle sizes, which results in a lower differential pressure. Considering that the injection rate is kept constant in our simulations, the pressure difference can indicate the permeability of the sealing zone, so finer particles can form a tighter sealing zone. The final flow rate and cumulative fluid loss volume change slightly as the particle size varies. However, $d_p = 0.2 W_{fi}$ and $d_p = 1.0 W_{fi}$ have a larger flow rate and cumulative fluid loss than the other particle sizes, as no complete sealing zone

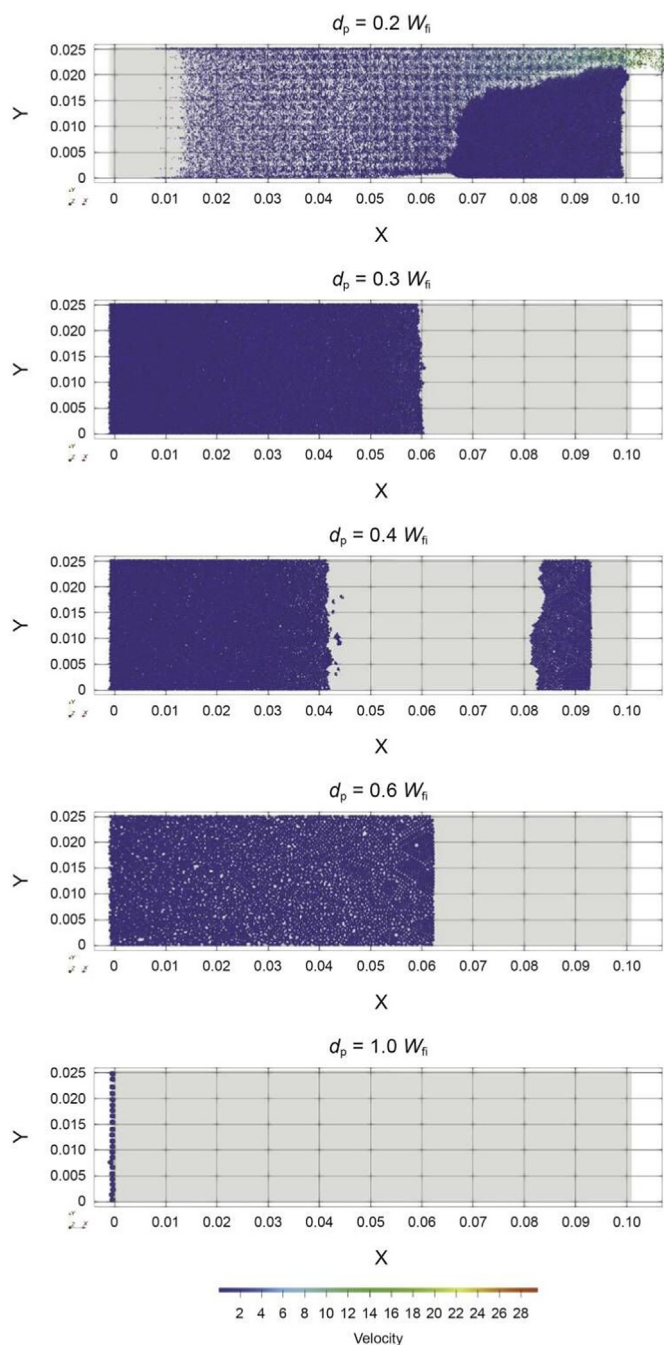


Fig. 8. Final fracture sealing state of LCMs under different ratios of LCM particle diameter to fracture inlet width after approximately $10 V_{fracture}$ drilling fluid is injected.

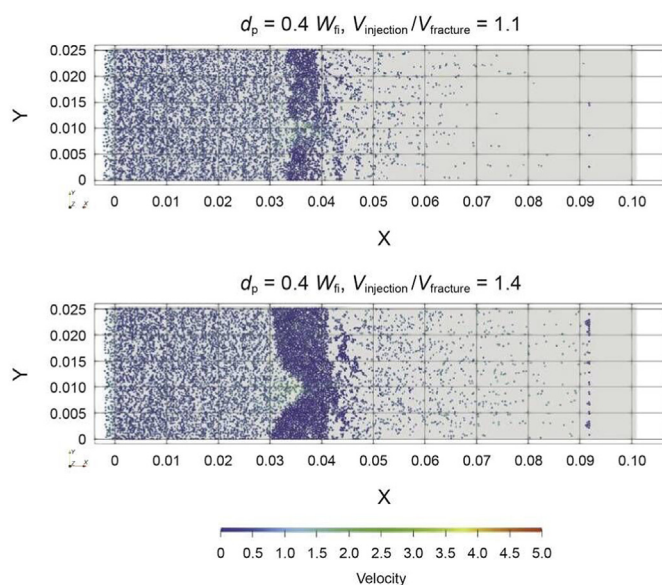


Fig. 9. Formation and evolution of the sealing zone by LCM particles with a size of $d_p = 0.4 W_{fi}$.

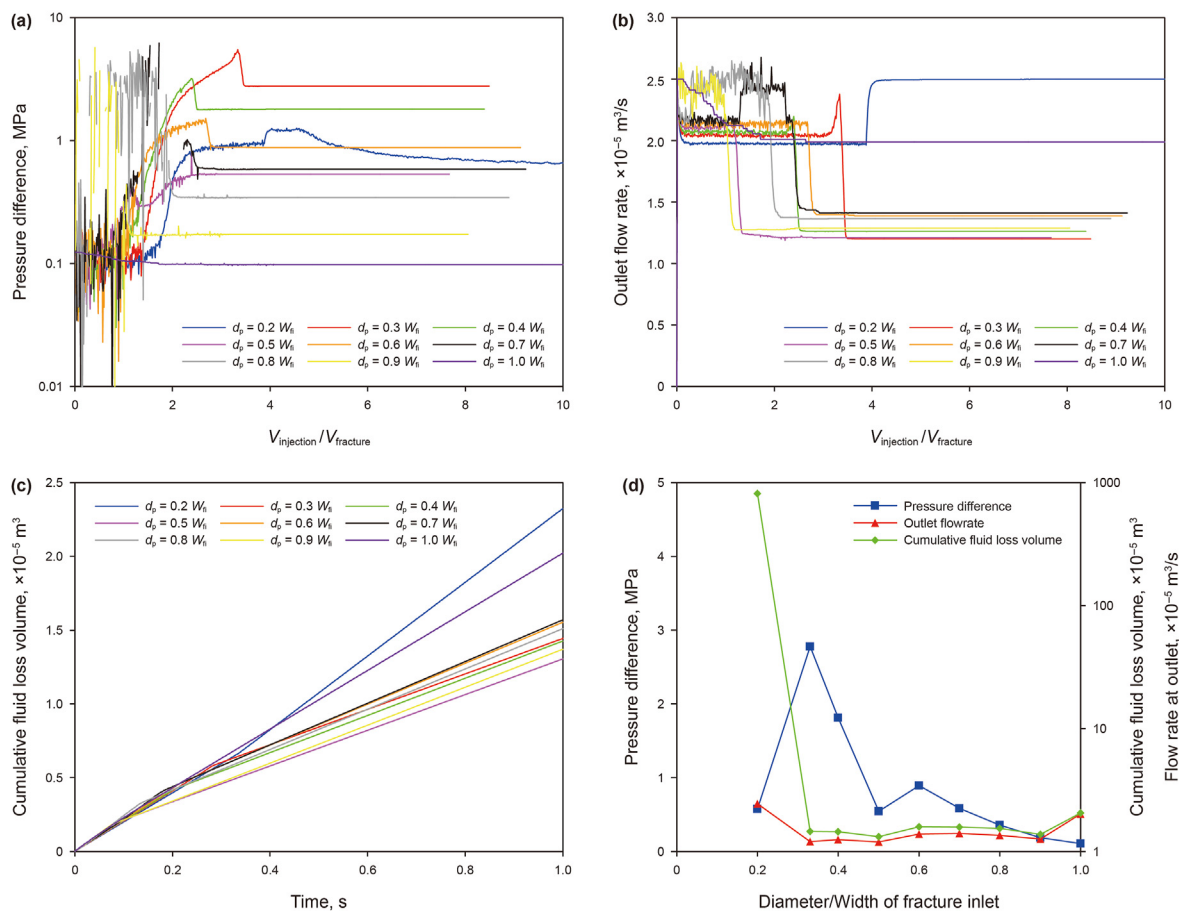


Fig. 10. Effect of LCM diameter to fracture inlet width ratio on the flow parameters inside the fracture: (a) pressure difference; (b) outlet flow rate; (c) cumulative drilling fluid loss volume; and (d) flow parameter at the final state.

formed.

The thermal degradation can reduce the particle size, which can increase the bridging time and the bridging depth. The bridging mechanism also switches from a single-particle bridging mechanism to a dual-particle bridging mechanism. However, the reduced particle size can form a tighter sealing zone.

4.3. Effect of thermally induced friction coefficient reduction on fracture sealing

The temperature increase causes the friction coefficient (f) reduction, which affects the LCM transport behavior, as shown in Fig. 11. Initially, different friction coefficients lead to similar LCM transport behavior. By the time $0.2 V_{fracture}$ drilling fluid is injected into the fracture, the transport and bridging behaviors differ from earlier times. All LCM particles flow out through the fracture, and no significant bridging zone forms for frictionless particles ($f = 0$) during the simulation period (Fig. 11, the first figure). For $f = 0.2$, a short bridging zone with a hole forms in the middle of the bridge in the fracture. The coming particles try to fill this gap (Fig. 11, the second figure). However, this bridge is unstable and collapses in the middle region as more LCM particles follow and reach this position. As more particles arrive, the bridging zone forms again and collapses in the upper region. When all the particles are injected, the bridging zone collapses from top to bottom and finally disappears (Fig. 12). For $f \geq 0.4$, the bridging zone also experiences collapse in the middle, and a significant bridging zone forms after more particles are injected. The length of the bridging zone for the friction

coefficient $f = 0.4$ is smaller than that of the friction coefficient of 0.6–1.0, which form similar bridges. Finally, no sealing zone forms for frictionless ($f = 0$) and low-friction ($f = 0.2$) particles. A seal with a similar shape and a slightly different depth forms for $f \geq 0.4$ (Fig. 11, the last three figures).

The friction coefficient has a significant effect on the quality of the sealing zone. The pressure difference increases as the friction coefficient decreases from 1 to 0.4. This indicates that the sealing zone becomes tighter against fluid flow. The pressure difference dramatically reduces at low friction values ranging from 0.4 to 0. The flow rate at the end and cumulative fluid loss volume change slightly when the friction coefficient decreases from 1 to 0.4. The flow rate and cumulative fluid loss volume increase sharply at $f = 0.2$ and $f = 0$ (Fig. 13).

In summary, the friction coefficient reduction increases the time of sealing zone formation and reduces the sealing probability and stability. For successful fracture sealing, a lower friction coefficient leads to a tighter sealing zone because low friction means low resistance of particles moving within a formed sealing zone, so particles are pushed by fluid drag to pack tighter but not enough to collapse the sealing zone.

4.4. Effect of thermally induced Young's modulus reduction on fracture sealing

The Young's modulus (E) of the LCM affects the formation of seals, as shown in Figs. 14–15. There are two different processes of seal formation for various Young's modulus. For Young's modulus,

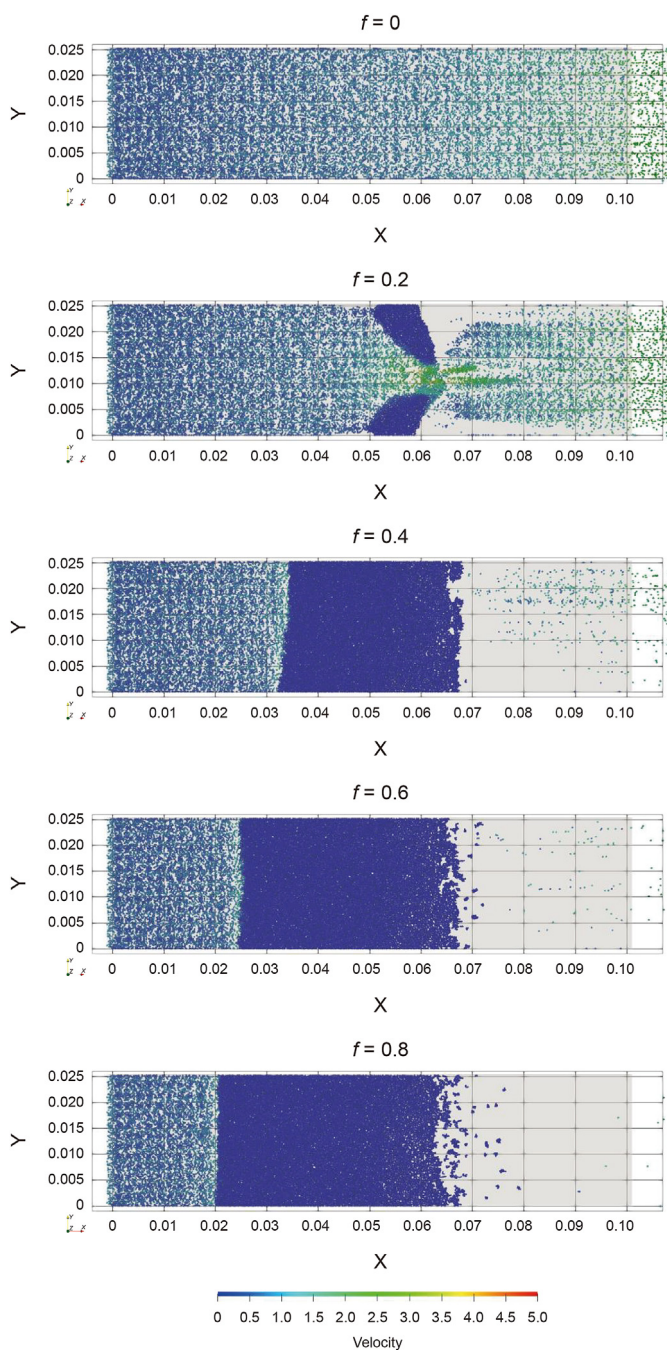


Fig. 11. Effect of LCM particle friction coefficient on the fracture sealing process. The snapshots show the LCM particles after approximately $2.5 V_{fracture}$ drilling fluid is injected. No sealing zone forms for $f = 0$, a dynamic gap forms in the sealing zone for $f = 0.2$, and a stable sealing zone forms for $f \geq 0.4$. The lower the friction coefficient is, the deeper the bridging position and the longer the sealing zone are.

$E \geq 1$ GPa (rigid LCMs, such as calcium carbonate), similar transport and bridging behavior of LCM particles are observed for Young's modulus of 1–100 GPa. The LCM particles bridge in a short time and form a sealing zone, expanding from the bridging position to the fracture inlet (Fig. 14). The final sealing zones are also similar in geometry. However, the sealing zone depth for $E = 1$ GPa is slightly deeper than the others. On the other hand, for $E < 1$ GPa (elastic LCMs, such as rubber), the formation of the seal zone is different. LCM particles also bridge in a short time, but the formed bridging zone is unstable. The bridging zone undergoes several bridging-

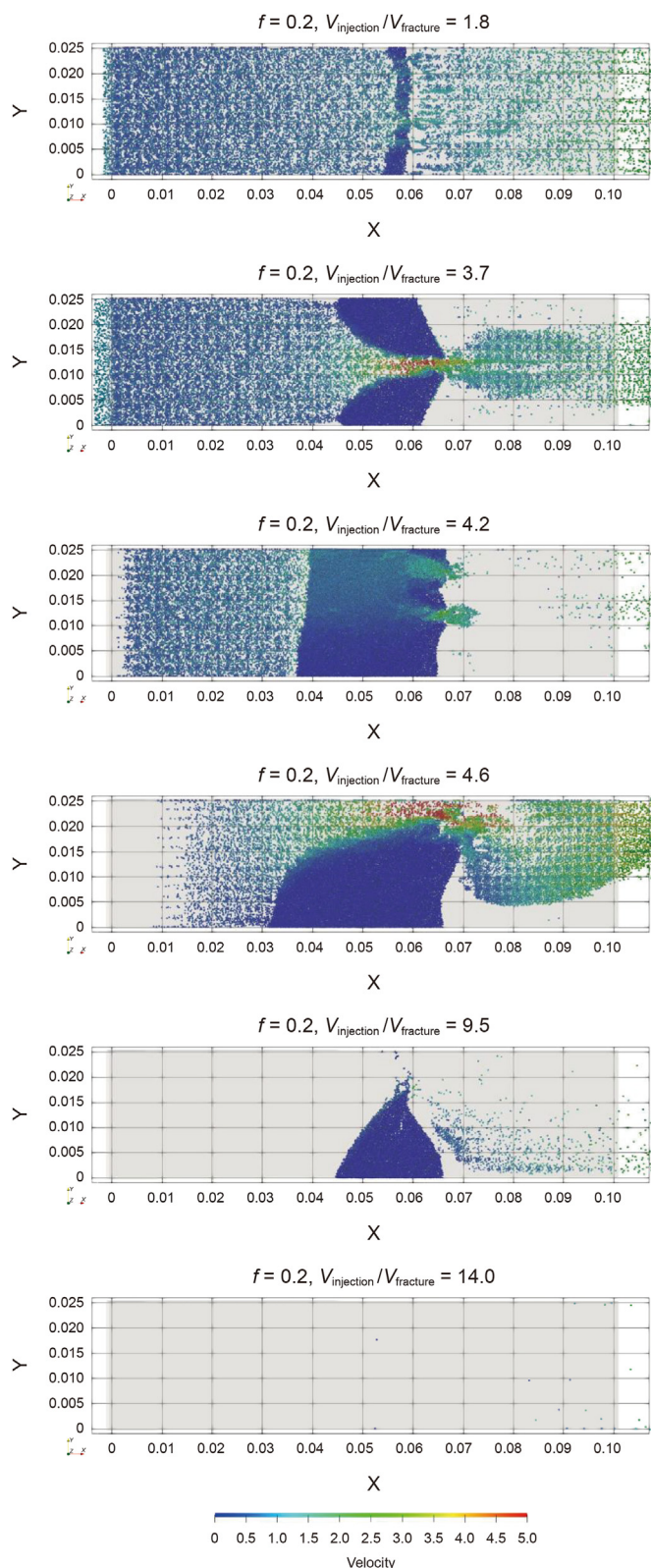


Fig. 12. Formation and instability of the sealing zone by LCM particles with a friction coefficient of $f = 0.2$. The snapshots show the LCM particles after different amounts of drilling fluid are injected. LCM particles bridge to form a seal at $V_{injection}/V_{fracture} = 1.8$. The seal is crushed and a gap forms in the middle of the sealing zone at $V_{injection}/V_{fracture} = 3.7$. The gap is filled and a thick but unstable sealing zone is formed at $V_{injection}/V_{fracture} = 4.2$. The sealing zone is crushed from the top due to the low friction coefficient at $V_{injection}/V_{fracture} = 4.6$. The residual sealing zone is crushed and disappears as more drilling fluid is injected at $V_{injection}/V_{fracture} = 9.5$ and $V_{injection}/V_{fracture} = 14.0$.

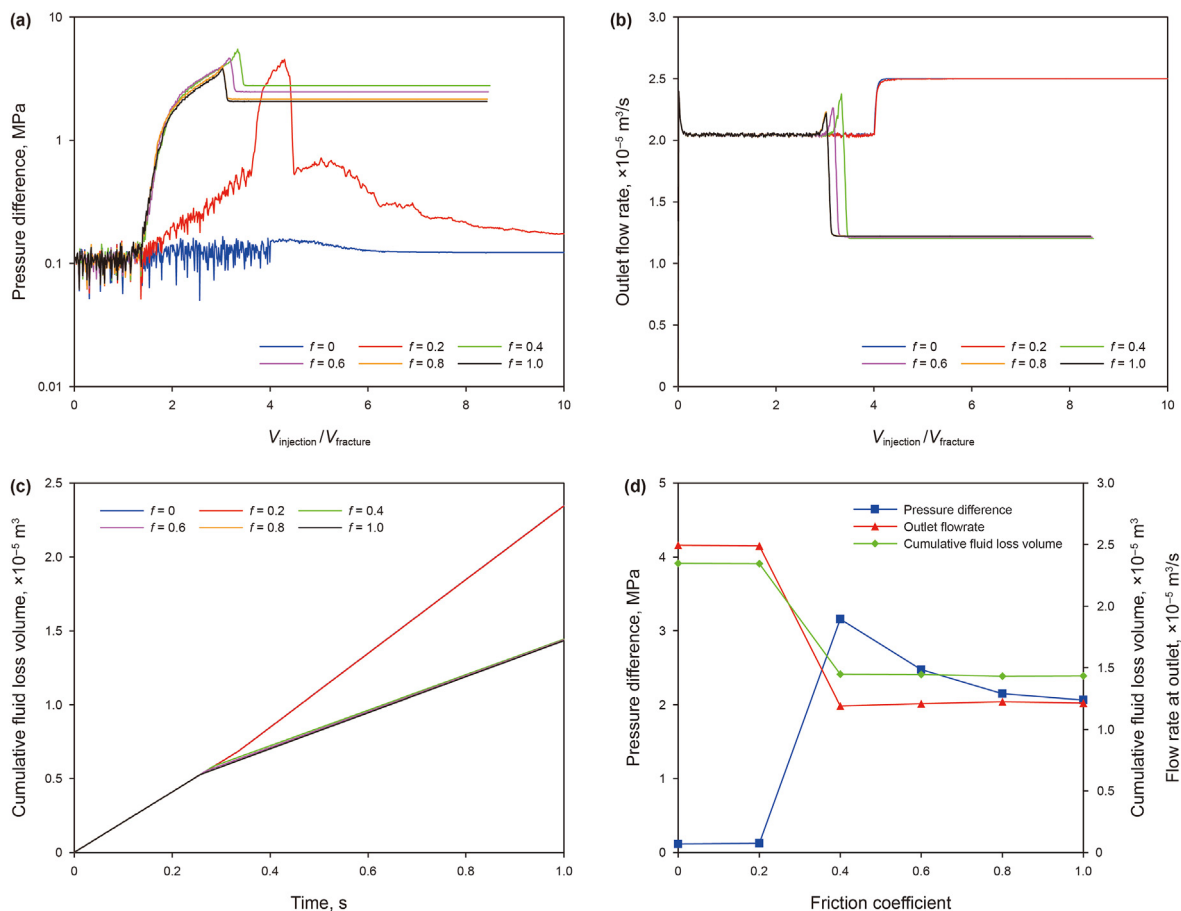


Fig. 13. Effect of LCM particle friction coefficient on the flow parameters inside the fracture: (a) pressure difference; (b) outlet flow rate; (c) cumulative drilling fluid loss volume; (d) flow parameter at the final state.

crushing-rebridging-recrushing cycles. A complete sealing zone does not form after all LCM particles flow out of the fracture (Fig. 15).

Young's modulus has little effect on the sealing zone quality. The pressure difference remains nearly constant for Young's modulus larger than 10 GPa. Then, it increases significantly at $E = 1$ GPa and finally drops to the smallest value near zero at $E = 0.1$ GPa. The flow rate and cumulative fluid loss volume change slightly as Young's modulus of the LCM particle decreases from 100 to 1 GPa. Then, a sharp drop in the flow rate and cumulative fluid loss volume occurs at $E = 0.1$ GPa (Fig. 16).

The simulation results show that the Young's modulus of the LCM particles has a weak influence on fracture sealing when the LCM is stiff, i.e., $E \geq 10$ GPa. For cases where Young's modulus decreases to 1 GPa, the seal forms further away from the inlet. However, soft LCMs with $E \leq 0.1$ GPa cannot seal the fracture.

4.5. Effect of thermally induced Poisson's ratio reduction on fracture sealing

The development of the sealing zone by LCM particles with Poisson's ratio equal to 0.3 is shown in Fig. 14. It is similar to the result of Poisson's ratio varying from 0.5 to 0.1. Therefore, the effect of Poisson's ratio on the formation of the sealing zone is negligible based on our simulation results.

Similarly, the effect of Poisson's ratio on the fracture sealing zone quality is also negligible. The pressure difference, flow rate and cumulative fluid loss volume change slightly as Poisson's ratio of the LCM particle varies from 0.5 to 0.1 (Fig. 17). Therefore,

Poisson's ratio does not affect fracture sealing by LCM particles.

4.6. Mechanisms behind the low efficiency of fracture sealing by LCMs at elevated temperatures

Now, we can summarize the reasons why fracture sealing by conventional LCMs at elevated temperatures usually fails. We can first assume a case where the conventional LCMs successfully seal the fracture and then discuss how it may fail at elevated temperatures. Fig. 18 summarizes the main mechanisms that lead to fracture sealing failure at elevated temperatures. In the case of deep/ultradeep well and geothermal well drilling, the wellbore temperature increases as the well drills deeper or drills into the geothermal reservoir. The properties of the drilling fluid and LCM may change significantly at elevated temperatures. Viscosity reduction of the drilling fluid and particle size degradation, strength reduction, Young's modulus reduction, Poisson's ratio reduction, and friction coefficient reduction of LCMs are some of these potential changes due to high temperatures that can affect the fracture sealing process.

Particle size degradation affects fracture sealing more than other effects. Particle size degradation comprises two aspects: reduction of the equivalent diameter and increase of sphericity. The particle size distribution of LCMs plays a vital role in fracture sealing, which directly affects particle bridging and the quality of the sealing zone. On the one hand, particle size degradation of the LCM reduces the particle size and concentration of the bridging particles. This is because larger bridging particles are more likely to be abraded (Kang et al., 2019a). Therefore, the size and concentration of

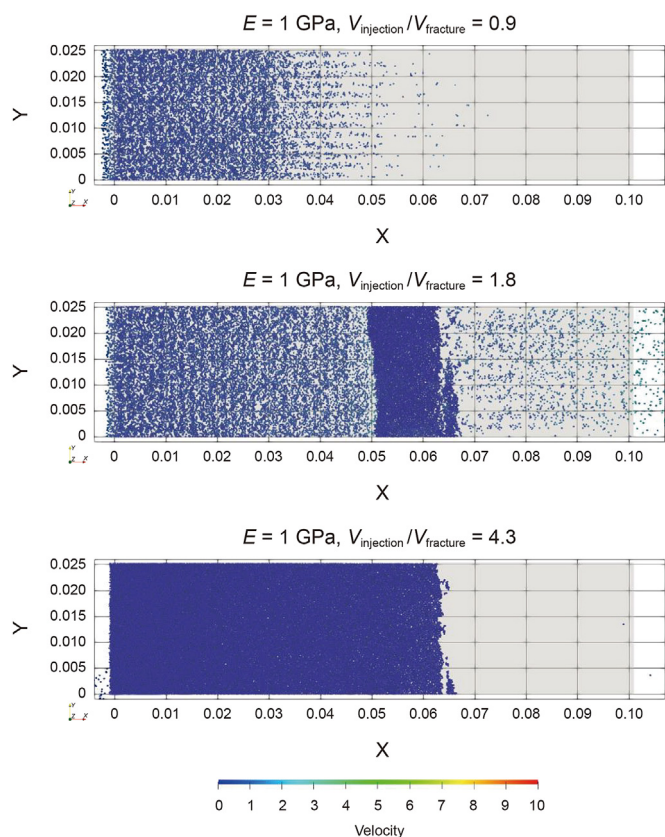


Fig. 14. Formation and evolution of the sealing zone by LCM particles with a Young's modulus of $E = 1$ GPa. The snapshots show the LCM particles after different amounts of drilling fluid are injected. LCM particles bridge and accumulate to form a sealing zone that extends to the fracture inlet as more drilling fluid flows. Similar results are obtained for $E = 10, 30, 50, 70$ and 100 GPa.

bridging particles do not satisfy bridging mechanisms, such as the “1/3 Bridge” theory (Abrams, 1977), “1/2–2/3 Bridge” principle (Luo and Luo, 1992), D90 rule (Hands et al., 1998), and ideal packing theory (Dick et al., 2000). As shown in Fig. 18 case (1), LCM particles cannot bridge until they move into a suitable narrow area in the deep parts of the fracture, which may cause formation damage at the pay zone. Large amounts of drilling fluid invade the formation via the fracture in the absence of timely bridging. The fracture may expand and propagate under large overbalanced pressures, and severe lost circulation occurs. On the other hand, the increase of sphericity makes the LCM particle transform from irregular to regular. The higher regularity of LCM particles makes them less likely to be captured by fractures (Xu et al., 2019b). Rounded bridging is more difficult and less likely to bridge a fracture. As a result of the two aspects of particle size degradation, the fracture width that can be sealed by a LCM slurry is reduced. Additionally, since the single-particle bridging mechanism changes to a dual-particle bridging mechanism and LCM particles become more regular as the particle size declines, the formed seal becomes less stable and easily blows away. Under high temperature and high shear conditions, rigid calcium carbonate-based LCMs (ground marble, etc.) have the largest particle size degradation, some shell LCMs (pecan hulls, etc.) have medium particle size degradation, elastic LCMs (resilient graphite, etc.) have small particle size degradation, and fiber LCMs (granular cellulose, etc.) have the smallest particle size degradation. Large bridging particles in LCMs are more prone to size degradation than small packing particles (Scott et al., 2012; Klungvedt and Saasen, 2022).

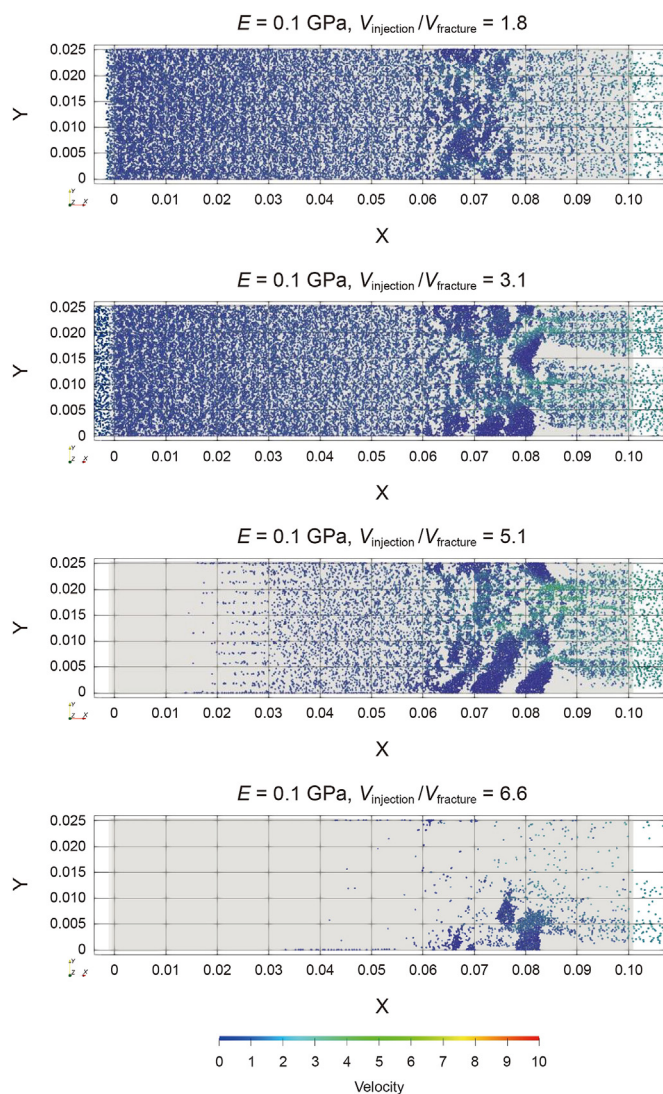


Fig. 15. Formation and instability of the sealing zone by LCM particles with a low Young's modulus of $E = 0.1$ GPa.

The friction coefficient is the key mechanical parameter of the LCM that affects both the fracture efficiency and sealing zone strength. A lower LCM friction coefficient leads to lower fracture sealing efficiency and lower fracture sealing strength (Xu et al., 2019a). The thermal effect and increased abrasion effect at elevated temperatures change the LCM particle from irregular to regular (more rounded) shapes. The higher sphericity of the particles results in a lower maximum static friction coefficient and an average sliding friction coefficient. Finally, the LCM particle is much more difficult to bridge inside the fracture. Even if the LCM particle forms a seal, the sealing zone may easily break down under slightly higher pressures. As the low LCM friction coefficient leads to a lower fracture sealing strength, the sealing zone can collapse from the middle region and eventually disappear (Fig. 18, case (2)). The friction coefficient of walnut shells decreases significantly under static high-temperature aging (Kang et al., 2019b). The friction coefficient of the gradually rounded calcium carbonate may also decrease under high temperature and high shear.

Young's modulus and Poisson's ratio are both essential mechanical properties of LCMs. Elevated temperatures result in a reduced Young's modulus and Poisson's ratio of the LCM. Reducing

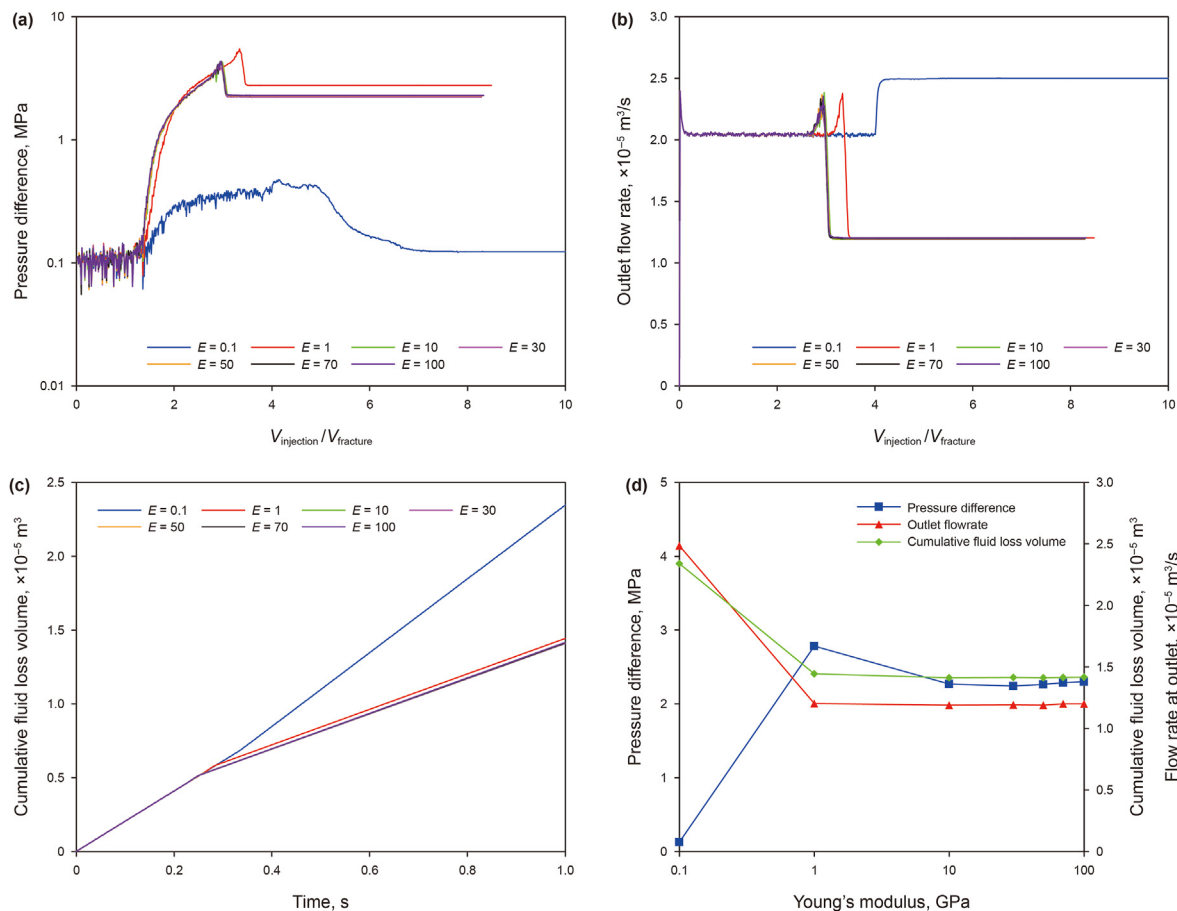


Fig. 16. Effect of LCM particle Young's modulus on the flow parameters inside the fracture: (a) pressure difference; (b) outlet flow rate; (c) cumulative drilling fluid loss volume; (d) flow parameter at the final state.

Poisson's ratio has no effect on fracture sealing based on the simulation results. Reducing Young's modulus means that the LCM undergoes more deformation under a given uniaxial stress. However, the reduction in Young's modulus has little effect on fracture sealing in the range of 10–100 GPa. When Young's modulus decreases to 1 GPa or lower, the bridging time and its corresponding depth increase until it cannot bridge (Fig. 18, case (3)). On the other

hand, for successful fracture sealing, a lower Young's modulus can lead to a tighter sealing zone, which can improve the sealing zone strength to some extent. This means that the elastic LCMs affect the formation and quality of the sealing zone at elevated temperatures. However, if the Young's modulus of LCMs decreases to a critical value at a very high temperature (such as the softening temperature in polymers), the sealing zone strength decreases. This is because a decreasing Young's modulus results in a decreasing strength and reduces the sealing zone strength by breaking the LCMs. At high temperature, shell LCMs are most likely to soften, and the elasticity of the elastic rubber LCM is significantly reduced. As shown in Fig. 1, the Young's modulus of calcium carbonate-based LCM (marble) also decreases significantly above 300 °C.

The drilling fluid viscosity variation has a different effect from other properties. The viscosity reduction of the drilling fluid promotes faster and shallower fracture sealing by the LCM particles (Fig. 18, case (4)). It also facilitates the formation of a plugging zone by increasing the filtration loss of the LCM slurry to the fracture surface. However, the viscosity reduction of the drilling fluid also makes the LCM particle settle quickly. As a result, the LCM particles settle in the bottom of the wellbore, and the concentration of the bridging LCM particles in the drilling fluid, which reaches the fracture, decreases. Consequently, the circulation of LCMs may not seal the fracture. Moreover, a lower drilling fluid viscosity will intensify the abrasion of LCM particles, which leads to a more significant particle size degradation (Kumar et al., 2013). Thus, the sealing zone may become difficult to form and easy to collapse. However, the comprehensive effect of both sides of the viscosity

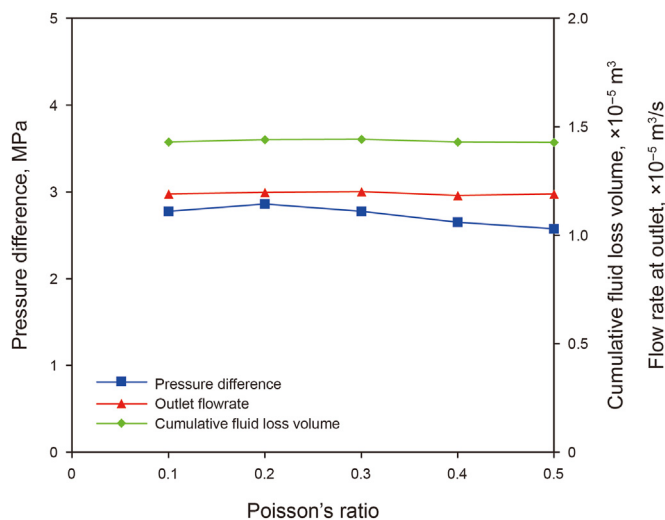


Fig. 17. Effect of LCM particle Poisson's ratio on the flow parameter inside the fracture.

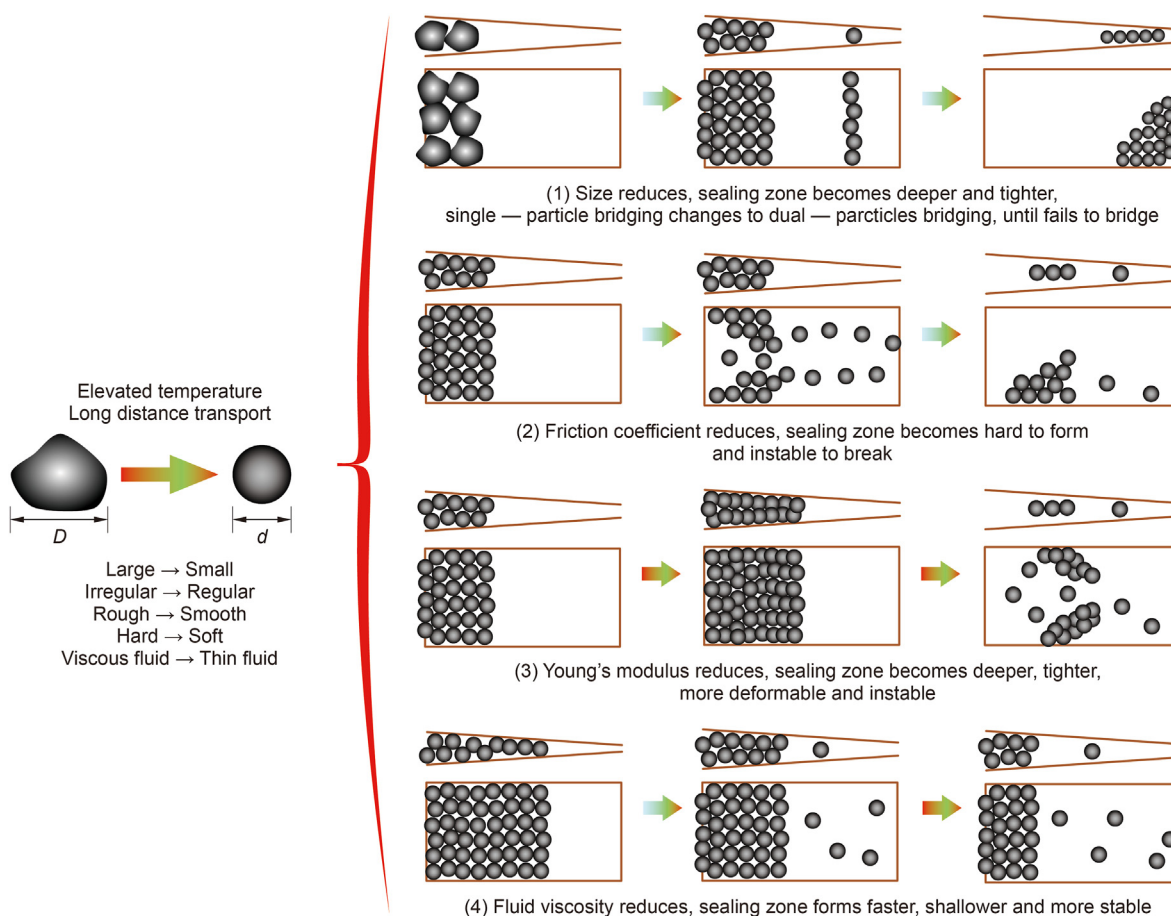


Fig. 18. Schematic illustration of low-efficiency fracture sealing by LCMs at an elevated temperature.

reduction of the drilling fluid on fracture sealing by LCMs needs further investigation.

5. Conclusions

In this study, a coupled CFD-DEM model is developed to simulate the behavior of granular LCMs in sealing a vertical wedge-shaped fracture. The variations in drilling fluids and LCMs at elevated temperatures are summarized and incorporated into the model. The fracture sealing process by LCM particles is simulated using various parameters for the drilling fluid and LCMs.

The results show that elevated temperature usually leads to a degradation of the size, strength and friction coefficient of LCMs and a reduction in drilling fluid viscosity. These variations have significant effects on the formation and stability of the sealing zone in a fracture. The reduction in particle size, friction coefficient and Young's modulus of LCMs at elevated temperatures results in a lower bridging probability, slower bridging initiation, deeper sealing depth, and tighter but unstable sealing zone. The bridging mechanism also changes from single-particle bridging to dual-particle bridging as the particle size decreases. However, the reduction in Poisson's ratio shows a negligible effect on fracture sealing. On the other hand, the reduction in drilling fluid viscosity makes the sealing zone form faster and shallower inside the fracture. As a result of the combined effect of variations in drilling fluid and LCM properties at elevated temperatures, a successful fracture sealing case by conventional LCMs may become unstable and even completely fail at elevated temperatures. To further understand the effect of high temperature on fracture sealing performance, future work needs to focus on more types of LCMs, the complex effect of

drilling fluid viscosity, and the plugging zone instability under long-term high-temperature conditions.

Declaration of competing interest

The authors declare that they have no known competing financial interests or personal relationships that could have appeared to influence the work reported in this paper.

Acknowledgment

The authors gratefully acknowledge the financial support from the National Natural Science Foundation of China (Grant No. 52274009), China Postdoctoral Science Foundation (Grant No. 2022M723501) and Science and Technology Planning Project of Sichuan Province (Grant No. 2021YJ0359).

References

- Abrams, A., 1977. Mud design to minimize rock impairment due to particle invasion. *J. Petrol. Technol.* 29, 586–592. <https://doi.org/10.2118/5713-PA>.
- Alsaba, M., Nygaard, R., Hareland, G., et al., 2014a. Review of Lost Circulation Materials and Treatments with an Updated Classification. *AADE National Technical Conference and Exhibition*. 15–16 April, Houston, Texas, USA.
- Alsaba, M., Nygaard, R., Saasen, A., et al., 2014b. Laboratory evaluation of sealing wide fractures using conventional lost circulation materials. In: *SPE Annual Technical Conference and Exhibition*. 27–29 October, Amsterdam, The Netherlands. <https://doi.org/10.2118/170576-ms>.
- Amani, M., Al-jubouri, M., 2012. An experimental investigation of the effects of ultra-high pressure and temperature on the rheological properties of water-based drilling fluids. In: *SPE/APPEA International Conference on Health, Safety, and Environment in Oil and Gas Exploration and Production*. 11–13 September, Perth, Australia. <https://doi.org/10.2118/157219-MS>.

- Avci, E., Mert, B.A., 2019. The Rheology and performance of geothermal spring water-based drilling fluids. *Geofluids* 2019, 3786293. <https://doi.org/10.1155/2019/3786293>.
- Bao, D., Qiu, Z.S., Qiu, W.Q., et al., 2019a. Experiment on properties of lost circulation materials in high temperature formation. *Acta Pet. Sin.* 40 (7), 846–857. <https://doi.org/10.7623/syxb201907009> (in Chinese).
- Bao, D., Qiu, Z.S., Zhao, X., et al., 2019b. Experimental investigation of sealing ability of lost circulation materials using the test apparatus with long fracture slot. *J. Pet. Sci. Eng.* 183, 106396. <https://doi.org/10.1016/j.petrol.2019.106396>.
- Blais, B., Lassaingne, M., Goniva, C., et al., 2016. Development of an unresolved CFD-DEM model for the flow of viscous suspensions and its application to solid-liquid mixing. *J. Comput. Phys.* 318, 201–221. <https://doi.org/10.1016/j.jcp.2016.05.008>.
- Brotóns, V., Tomás, R., Ivorra, S., et al., 2013. Temperature influence on the physical and mechanical properties of a porous rock: san Julian's calcarenite. *Eng. Geol.* 167, 117–127. <https://doi.org/10.1016/j.enggeo.2013.10.012>.
- Carrier III, W.D., 2003. Goodbye, hazen; hello, kozeny-carman. *J. Geotech. Geoenviron. Eng.* 129, 1054–1056. [https://doi.org/10.1061/\(ASCE\)1090-0241\(2003\)129:11\(1054\)](https://doi.org/10.1061/(ASCE)1090-0241(2003)129:11(1054)).
- Chakraborti, R.K., Kaur, J., 2014. Noninvasive measurement of particle-settling velocity and comparison with Stokes' Law. *J. Environ. Eng.* 140, 4013008. [https://doi.org/10.1061/\(ASCE\)EE.1943-7870.0000790](https://doi.org/10.1061/(ASCE)EE.1943-7870.0000790).
- Concha, A.F., 2009. Settling velocities of particulate systems. *Kona Powder Part. J.* 27, 18–37. <https://doi.org/10.14356/kona.2009006>.
- Crowe, C.T., Schwarzkopf, J.D., Sommerfeld, M., et al., 2011. *Multiphase Flows with Droplets and Particles*, second ed. CRC Press, Boca Raton. <https://doi.org/10.1201/b11103>.
- Di Felice, R., 1994. The voidage function for fluid-particle interaction systems. *Int. J. Multiphas. Flow* 20, 153–159. [https://doi.org/10.1016/0301-9322\(94\)90011-6](https://doi.org/10.1016/0301-9322(94)90011-6).
- Dick, M.A., Heinz, T.J., Svoboda, C.F., et al., 2000. Optimizing the selection of bridging particles for reservoir drilling fluids. In: 2000 SPE International Symposium on Formation Damage. 23–24 February, Lafayette, Louisiana, USA. <https://doi.org/10.2118/58793-MS>.
- Ettehad, A., Tezcan, M., Altun, G., 2019. A comparative study on essential parameters to minimize sealing time in wide fractures. *J. Pet. Sci. Eng.* 183, 106422. <https://doi.org/10.1016/j.petrol.2019.106422>.
- Ergun, S., 1952. Fluid flow through packed columns. *Chem. Eng. Prog.* 48, 89–94.
- Feng, Y., Li, G., Meng, Y.F., et al., 2018. A novel approach to investigating transport of lost circulation materials in rough fracture. *Energies* 11, 2572. <https://doi.org/10.3390/en1102572>.
- Finger, J., Blankenship, D., 2010. *Handbook of Best Practices for Geothermal Drilling*. Sandia National Laboratories, Albuquerque.
- Grant, P., Lassus, L., Savari, S., et al., 2016. Size degradation studies of lost circulation materials in a flow loop. In: IADC/SPE Drilling Conference and Exhibition. 1–3 March, Fort Worth, Texas, USA. <https://doi.org/10.2118/178774-MS>.
- Hager, A., 2014. *CFD-DEM on Multiple Scales - an Extensive Investigation of Particle-Fluid Interactions*. Ph.D. Dissertation. Johannes Kepler University Linz.
- Hager, A., Kloss, C., Goniva, C., 2018. Combining open source and easy access in the field of DEM and coupled CFD-DEM: LIGGGHTS®, CFDEM®coupling and CFDEM®workbench. In: 28th European Symposium on Computer Aided Process Engineering. 10–13 June, Graz, Austria. <https://doi.org/10.1016/B978-0-444-64235-6.50296-5>.
- Hands, N., Kowbel, K., Maikranz, S., et al., 1998. Drill-in fluid reduces formation damage, increases production rates. *Oil Gas J.* 96, 65–69.
- Jeennakorn, M., Alsaba, M., Nygaard, R., et al., 2019. The effect of testing conditions on the performance of lost circulation materials: understandable sealing mechanism. *J. Pet. Explor. Prod. Technol.* 9, 823–836. <https://doi.org/10.1007/s13202-018-0550-4>.
- Kaageson-Loe, N., Sanders, M.W., Growcock, F., et al., 2009. Particulate-based loss-prevention material-The secrets of fracture sealing revealed. *SPE Drill. Complet.* 24, 581–589. <https://doi.org/10.2118/112595-pa>.
- Kang, Y.L., Tan, Q.G., You, L.J., et al., 2019a. Experimental investigation on size degradation of bridging material in drilling fluids. *Powder Technol.* 342, 54–66. <https://doi.org/10.1016/j.powtec.2018.09.086>.
- Kang, Y.L., Wang, K.C., Xu, C.Y., et al., 2019b. High-temperature aging property evaluation of lost circulation materials in deep and ultra-deep well drilling. *Acta Pet. Sin.* 40, 215–223. <https://doi.org/10.7623/syxb201902010> (in Chinese).
- Kloss, C., Goniva, C., Hager, A., et al., 2012. Models, algorithms and validation for opensource DEM and CFD-DEM. *Prog. Comput. Fluid Dynam. Int. J.* 12, 140–152. <https://doi.org/10.1504/PCFD.2012.047457>.
- Klungtvedt, K.R., Saasen, A., 2022. Comparison of lost circulation material sealing effectiveness in water-based and oil-based drilling fluids and under conditions of mechanical shear and high differential pressures. *J. Energy Resour. Technol.* 144 (12), 123011.
- Kumar, A., Chellappah, K., Aston, M., et al., 2013. Quality control of particle size distributions. In: SPE European Formation Damage Conference and Exhibition. 5–7 June, Noordwijk, The Netherlands. <https://doi.org/10.2118/165150-MS>.
- Lapple, C.E., Shepherd, C.B., 1940. Calculation of particle trajectories. *Ind. Eng. Chem.* 32, 605–617.
- Lin, C., Taleghani, A.D., Kang, Y.L., et al., 2022. A coupled CFD-DEM simulation of fracture sealing: effect of lost circulation material, drilling fluid and fracture conditions. *Fuel* 322, 124212. <https://doi.org/10.1016/j.fuel.2022.124212>.
- Loeppeke, G.E., Glowka, D.A., Wright, E.K., 1990. Design and evaluation of lost-circulation materials for severe environments. *J. Petrol. Technol.* 42, 328–337. <https://doi.org/10.2118/18022-PA>.
- Luo, X.D., Luo, P.Y., 1992. Study on the application of shielding temporary plugging technique in reservoir protection. *Drill. Fluid Complet. Fluid* 9, 19–27 (in Chinese).
- Norouzi, H.R., Zarghami, R., Sotudeh-Gharebagh, R., et al., 2016. *Coupled CFD-DEM Modeling: Formulation, Implementation and Application to Multiphase Flows*. John Wiley & Sons, Chichester.
- Nugroho, W.A., Hermawan, S., Lazuardi, B.H., et al., 2017. Drilling problems mitigation in geothermal environment, case studies of stuck pipe and lost circulation. In: SPE/IATMI Asia Pacific Oil & Gas Conference and Exhibition. 17–19 October, Jakarta, Indonesia. <https://doi.org/10.2118/186922-MS>.
- Peng, Z., Doroodchi, Elham, Luo, C., et al., 2015. Influence of void fraction calculation on fidelity of CFD-DEM simulation of gas-solid bubbling fluidized beds. *AIChE J.* 61, 857–866. <https://doi.org/10.1002/aic>.
- Pierce, K.G., Livesay, B.J., 1994. *A Study of Geothermal Drilling and the Production of Electricity from Geothermal Energy*. Sandia Report, Albuquerque.
- Pota, J., Bancewicz, M., Koza, Z., 2017. Is Magnus effect relevant for proppant settling in narrow fractures? *Energy Proc.* 125, 443–449. <https://doi.org/10.1016/j.egypro.2017.08.097>.
- Rushd, S., Hassan, I., Sultan, R.A., et al., 2019. Terminal settling velocity of a single sphere in drilling fluid. *Part. Sci. Technol.* 37 (8), 943–952. <https://doi.org/10.1080/02726351.2018.1472162>.
- Santoyo, E., Santoyo-Gutiérrez, S., Garcóa, A., et al., 2001. Rheological property measurement of drilling fluids used in geothermal wells. *Appl. Therm. Eng.* 21, 283–302. [https://doi.org/10.1016/S1359-4311\(00\)00003-X](https://doi.org/10.1016/S1359-4311(00)00003-X).
- Savari, S., Whitfill, D.L., Kumar, A., 2012. Resilient lost circulation material (LCM): a significant factor in effective wellbore strengthening. In: SPE Deepwater Drilling & Completions Conference. 20–21 June, Galveston, Texas, USA. <https://doi.org/10.2118/153154-MS>.
- Scott, P.D., Beardmore, D.H., Wade, Z.L., et al., 2012. Size degradation of granular lost circulation materials. In: IADC/SPE Drilling Conference and Exhibition. 6–8 March, San Diego, California, USA. <https://doi.org/10.2118/151227-MS>.
- Sun, Z., Balhoff, M.T., Espinoza, D.N., 2018. *Fluid Injection Induced Fracture Initiation Based on a Resolved CFD-DEM Approach*. 52nd U.S. Rock Mechanics/Geomechanics Symposium. 17–20 June, Seattle, Washington, USA.
- Valsecchi, P., 2014. On the shear degradation of lost circulation materials. *SPE Drill. Complet.* 29, 323–328. <https://doi.org/10.2118/163512-PA>.
- Visser, C., Eustes III, A.W., Baker, W., et al., 2014. *Geothermal Drilling and Completions: Petroleum Practices Technology Transfer*. National Renewable Energy Laboratory, Golden.
- Wang, F.H., Tan, X.C., Wang, R.H., et al., 2012. High temperature and high pressure rheological properties of high-density water-based drilling fluids for deep wells. *Petrol. Sci.* 9, 354–362. <https://doi.org/10.1007/s12182-012-0219-4>.
- Wellmann, C., Lillie, C., Wriggers, P., 2008. Comparison of the macroscopic behavior of granular materials modeled by different constitutive equations on the microscale. *Finite Elem. Anal. Des.* 44, 259–271. <https://doi.org/10.1016/j.finel.2007.11.007>.
- Xu, C.Y., Yan, X.P., Kang, Y.L., et al., 2019a. Friction coefficient: a significant parameter for lost circulation control and material selection in naturally fractured reservoir. *Energy* 174, 1012–1025. <https://doi.org/10.1016/j.energy.2019.03.017>.
- Xu, C.Y., Zhang, J.Y., Kang, Y.L., et al., 2019b. Investigation on the transport and capture behaviours of lost circulation material in fracture with rough surface. In: International Petroleum Technology Conference. 26–28 March, Beijing, China. <https://doi.org/10.2523/IPTC-19571-MS>.
- Yan, J.N., Zhao, X.H., 2003. Rheological properties of oil-based drilling fluids at high temperature and high pressure. *Acta Pet. Sin.* 24 (3), 104–109. <https://doi.org/10.7623/syxb200303023> (in Chinese).
- Yang, L., 2015. *Comparative Analysis of Lost Circulation Material Particle Size and Degradation in Drilling Fluids*. The University of Texas at Austin.
- Zhang, L., Mao, X., Lu, A., 2009. Experimental study on the mechanical properties of rocks at high temperature. *Sci. China, Ser. A: Technol. Sci.* 52, 641–646. <https://doi.org/10.1007/s11431-009-0063-y>.
- Zhao, S.Y., Yan, J.N., Shu, Y., et al., 2008. Rheological properties of oil-based drilling fluids at high temperature and high pressure. *J. Cent. South Univ. Technol. (Engl. Ed.)* 15, 457–461. <https://doi.org/10.1007/s11771-008-0399-7>.
- Zhou, Z.Y., Kuang, S.B., Chu, K.W., et al., 2010. Discrete particle simulation of particle-fluid flow: model formulations and their applicability. *J. Fluid Mech.* 661, 482–510. <https://doi.org/10.1017/S002211201000306X>.
- Zhu, W.X., Zheng, X.H., Li, G.M., 2020. Micro-bubbles size, rheological and filtration characteristics of Colloidal Gas Aphron (CGA) drilling fluids for high temperature well: role of attapulgite. *J. Pet. Sci. Eng.* 186, 106683. <https://doi.org/10.1016/j.petrol.2019.106683>.